RESEARCH PAPER

PCCP
www.rsc.org/pccp

Light stability of pyrazolotriazole azamethine dyes at oil/aqueous interfaces

Chetan K. Parmar,*[a] Garry Rumbles†[a] and Christopher J. Winscom[b]

[a] *Department of Chemistry, Imperial College, London, UK SW7 2AY. E-mail: ck_parmar@yahoo.co.uk*
[b] *Kodak European Research, Headstone Drive, Harrow, UK HA1 4TY*

Received 7th December 2004, Accepted 25th February 2005
First published as an Advance Article on the web 14th March 2005

Film and dispersion coatings of two pyrazolotriazole azamethine (PT) dyes are used to study the effect of increasing the surface-area-to-volume (SA : V) ratio of the oil/aqueous (solvent/gelatin) interface on non-oxidative and oxidative fade characteristics. High concentration solutions of the dyes in a poly(vinyl acetate)–dicyclohexylphthalate mixture as solvent are coated on glass substrates with a gelatin overcoat to produce thin film coatings and are also dispersed in gelatin to create "oil-in-gelatin" dispersion coatings. It is calculated that the dispersion coatings possess a SA : V ratio of approximately 20× greater than the film coatings. In non-oxidative fade conditions both the film and dispersion samples possess similar quantum yields of fade, implying that the presence of a solvent/gelatin interface does not significantly affect any electron transfer fade mechanisms. However, in oxidative fade conditions increasing the SA : V ratio of the interface by 20× leads to an increase in the quantum yield of fade of only a factor of 1.5–2. This disproportionate increase in the fade kinetics in dispersion coatings is explained by a kinetic scheme modelling oxygen diffusion through the coatings. It shows that the rate determining step for dye fade starts to become the diffusion of oxygen through the air/gelatin interface, and explains why changes in the SA : V ratio are not fully transferred to the quantum yield of fade.

Introduction

The light stability of colour photographs has received much interest from the imaging technology community.[1–3] Modern colour photography is based on the subtractive process, whereby layers of yellow, magenta and cyan azamethine dyes are used to record three colour components of an image.[4] Historically, the azamethine dyes used in the magenta record possess poor light stability relative to those used in cyan and yellow, and much photophysical and photochemical work has been carried out to try to explain this.[5–9]

In a particular colour layer of an exposed and fully developed multilayer photographic coating, the dyes reside at fractional molar concentrations in oleophilic droplets of diameters on a sub-micron level. Prior to processing, these droplets, which are dispersed in gelatin using a suitable surfactant, contain the corresponding dye couplers (precursors). Therefore upon processing, these conditions lead to a significant proportion of dye molecules at the interface between the oleophilic droplet and aqueous gelatin. There are several ways that this interface can induce photophysical changes to the dye molecules in its vicinity. These include changes in dielectric constant, local viscosity, and concentrations of active species capable of causing changes to the dye structure—such species include protons and hydroxyl ions.

Previous work has shown that the molecular photophysical properties of magenta pyrazolotriazole azamethine (PT) dyes are significantly affected by both the dielectric constant and viscosity of the solvent, with the latter promoting a rigidisation of the dye.[10–12] Two typical PT dye examples are shown in Fig. 1: dye A, which is a 7*H*-pyrazolo[1,5-*b*][1,2,4]triazole azamethine dye, and dye B, which is a 7*H*-pyrazolo[5,1-*c*][1,2,4]triazole azamethine dye.

By dissolving dyes A and B (10 μM) in surfactant (Triton X-100)–buffer solutions ranging from pH 3 to 10, we have noted that changes in proton and hydroxyl concentration have little effect on the photophysical properties. However, in a previous article we modelled experimentally the oil/aqueous interface and observed the formation of luminescent aggregates of both dyes A and B at solution/hydrated glass interfaces, caused by rigidisation and adsorption of the dye molecules at the interface.[12]

In this article we discriminate between the light stability of those dye molecules in the bulk oleophilic droplet and those residing at the interface and look further at the effect of oxidative and non-oxidative conditions on the fade characteristics of the dyes in these different environments.

Light fade

The loss of dye can be initiated both chemically and photochemically. Since only the latter is being studied, the quantum yield of fade, ϕ_{fade}, can be defined as

$$\phi_{\text{fade}} = \frac{k_{\text{loss}}}{I_{\text{a}}} \tag{1}$$

where k_{loss} is the rate of destruction of dye molecules and I_{a} is the rate of absorption of photons which is expressed as

$$I_{\text{a}} = \frac{1}{N_{\text{A}}} \int_{\lambda_1}^{\lambda_2} \frac{S_\lambda T_\lambda A_\lambda}{E_\lambda} \mathrm{d}\lambda \tag{2}$$

Here, N_{A} is Avagadro's constant, S_λ (W nm^{-1} cm^{-2}) is the spectral radiant flux of the light source per unit area, E_λ is the energy of a photon at wavelength λ, T_λ is the transmittance of any filters placed between the light source and sample, and

† Present address: National Renewable Energy Laboratory, 1617 Cole Boulevard, Golden, CO 80401-3393, USA.

DOI: 10.1039/b418363k

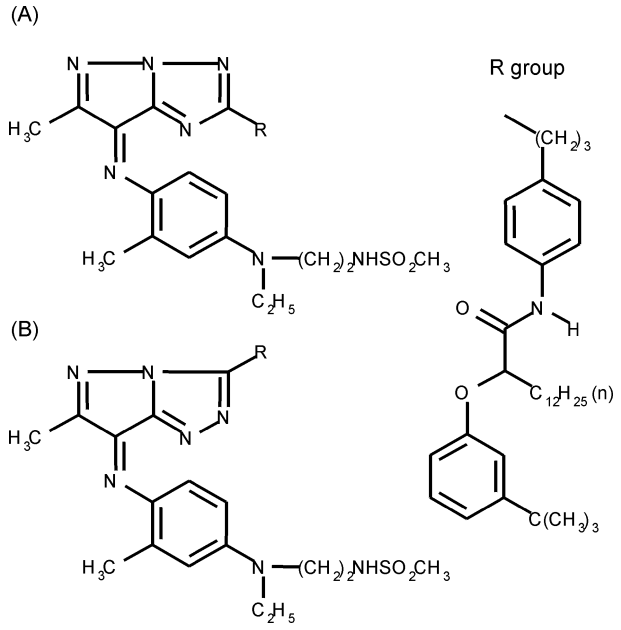

Fig. 1 The chemical structures of the two PT dyes.

A_λ is the amount of light absorbed by the sample, which is defined as

$$A_\lambda = 1 - 10^{-\mathrm{Abs}} \tag{3}$$

where Abs is the absorbance of the sample.

k_{loss} can be determined by measuring k_{Abs}, the rate of loss of absorbance per unit area of sample, and prior knowledge of the maximum molar decadic absorption coefficient, $\varepsilon_{\max}$ ($\mathrm{M^{-1}\ cm^{-1}}$).

$$k_{\mathrm{loss}} = \frac{k_{\mathrm{Abs}}}{10^3 \varepsilon_{\max}} \tag{4}$$

Oxidative fade

The loss of dye through an oxidative light fade mechanism usually involves singlet oxygen, O_2 ($^1\Delta_g$). Electron-rich double bonds in conjugated polymer and polynuclear aromatic molecules are particularly prone to attack by this species. Practically all chromophores fall within these structural categories.[13] Eqns. (5)–(10) describe the self-oxidative fade mechanism of dye molecules (Dye) which generate singlet oxygen, O_2 ($^1\Delta_g$), from triplet oxygen, O_2 ($^3\Sigma_g^-$) through energy transfer with the dye possessing a singlet ground state to triplet energy difference, $\Delta E_{\mathrm{T-S}}$, of greater than 94.3 kJ $\mathrm{mol^{-1}}$.[14]

$$^1\mathrm{Dye} + h\nu \rightarrow {}^1\mathrm{Dye}^* \tag{5}$$

$$^1\mathrm{Dye}^* \xrightarrow{\mathrm{ISC}} {}^3\mathrm{Dye}^* \tag{6}$$

$$^3\mathrm{Dye}^* + \mathrm{O_2}(^3\Sigma_g^-) \xrightarrow{\mathrm{ET}} {}^1\mathrm{Dye} + \mathrm{O_2}(^1\Delta_g) \tag{7}$$

$$\mathrm{O_2}(^1\Delta_g) \rightarrow \mathrm{O_2}(^3\Sigma_g^-) \tag{8}$$

$$\mathrm{O_2}(^1\Delta_g) + {}^1\mathrm{Dye} \rightarrow \mathrm{O_2}(^3\Sigma_g^-) + {}^1\mathrm{Dye} \tag{9}$$

$$\mathrm{O_2}(^1\Delta_g) + {}^1\mathrm{Dye} \rightarrow \mathrm{PRODUCTS} \tag{10}$$

If $\Delta E_{\mathrm{T-S}}$ for the dye is close to or less than this energy barrier then quenching of $^1O_2$ can occur (eqn. (9)). This has been observed for pyrazolone and indoaniline azamethine dyes.[15,16] For PT dyes $\Delta E_{\mathrm{T-S}}$ lies in between 100 and 120 kJ $\mathrm{mol^{-1}}$ making this class of dye more prone to oxidative fade.[17,18]

Non-oxidative fade

We define non-oxidative fade as that which arises from excited state electron transfer processes and results in the net destruction of dye molecules. These processes can formally involve both oxidation and reduction through the loss or gain of electrons in the absence of oxygen and can be more complex than oxidative fade mechanisms. The dye molecule can act as an electron acceptor or donor to form a radical ion pair with another electron donor, ED, or acceptor, EA. This radical ion pair then disintegrates to destroy the dye.[6,19,20] It should be noted that ED and EA can also quench the excited state of the dye. Eqns. (11)–(14) summarise non-oxidative fade from the excited state (singlet or triplet) of Dye.

$$\mathrm{Dye}^* + \mathrm{ED} \rightarrow \mathrm{Dye}^{\bullet -}\ \mathrm{ED}^{\bullet +} \tag{11}$$

$$\mathrm{Dye}^* + \mathrm{EA} \rightarrow \mathrm{Dye}^{\bullet +}\ \mathrm{EA}^{\bullet -} \tag{12}$$

$$\mathrm{Dye}^{\bullet -}\ \mathrm{ED}^{\bullet +} \rightleftharpoons \mathrm{Dye}^{\bullet -} + \mathrm{ED}^{\bullet +} \rightarrow \mathrm{PRODUCTS} \tag{13}$$

$$\mathrm{Dye}^{\bullet +}\ \mathrm{EA}^{\bullet -} \rightleftharpoons \mathrm{Dye}^{\bullet +} + \mathrm{EA}^{\bullet -} \rightarrow \mathrm{PRODUCTS} \tag{14}$$

For azamethine dyes non-oxidative fade is most likely to occur from the singlet excited state, since the quantum yield of triplet state formation is very low.[21] In photographic coatings molecules that can act as electron donors/acceptors include residual components from photographic development such as the imaging dye precursors or impurities in the photographic material. Other ground state dye molecules within the vicinity of a photo-excited dye molecule can also act as electron donors /acceptors. It is difficult to isolate particular species responsible for the loss of dye. However, experiments performed on pyrazolone and PT dyes with specific electron donating species incorporated into dye solutions show that non-oxidative fade can be induced in these systems.[7]

It must be stressed that the occurrence of fade through distinct mechanistic pathways cannot be assumed. Aono *et al.* have studied the light stability of several azamethine dye classes in photographic media, and in particular, ways to inhibit oxidative fade mechanisms.[22] Their experiments showed that by enclosing the film with a transparent polymer coating, acting as a barrier to oxygen, the rate of fade is not suppressed but is in fact enhanced for some dye classes, indicating that non-oxidative fade mechanisms flourish in the absence of oxygen. This implies that oxidative and non-oxidative fade mechanisms compete with each other rather than acting co-operatively, and once one of these is inhibited, the other will prevail.

In this article we have performed experiments in two distinct conditions where non-oxidative and oxidative fade may individually thrive in the absence of the other. Strong light intensities and an inert nitrogen atmosphere are used to promote non-oxidative fade, and relatively weaker light intensities with normal atmospheric conditions are used to reduce the fade rate to a level that is controlled by the rate of diffusion of oxygen through the coatings.

Experimental

Fading apparatus

Non-oxidative fade. Light from a quartz-halogen lamp (General Electric, 15 V, 150 W, with dichroic reflector) was passed through several air-cooled heat-filters and channelled through a flexible liquid light pipe (Oriel, diameter 8 mm, length 1 m). The combination of filters and liquid light pipe remove high energy UV (<350 nm), and IR light (>730 nm).

The liquid light pipe entered a sample chamber (Fig. 2) and passed through a 5 mm aperture, with the optical surface of the light pipe positioned 3.5 mm away from the surface of the coating. Housed inside this gap were a gas-inlet to flush nitrogen at a constant rate (2 $\mathrm{dm^3\ min^{-1}}$) to create an

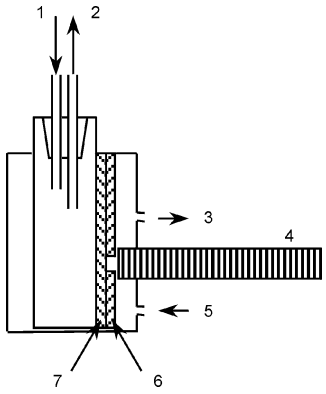

Fig. 2 Schematic diagram of sample chamber for non-oxidative fade experiments. (1) Water in. (2) Water Out. (3) Fibre optic to light dependent resistor. (4) Filtered light source through a liquid light pipe. (5) Nitrogen gas inlet. (6) Aperture (5 mm diameter). (7) Coating on surface of cuvette.

oxygen-free atmosphere around the sample, and also an optical fibre channelled to a CdS light dependent resistor (NORP12) to monitor the light intensity falling on the sample. During rapid fade, the voltage of the lamp was continually adjusted to maintain a constant resistance across the sensor. The temperature of the cuvette was thermostatically regulated at 24 °C by circulating distilled water through two syringe needles pierced through a Subaseal® stopper that sealed the top of the cuvette.

Absorption spectra were recorded at 30 min intervals on a Perkin-Elmer Lambda 5 spectrophotometer for a period of 4 h. During each absorption measurement the water circulator was switched off to minimise distortions to the background of the measured spectrum.

Oxidative fade

The high intensity daylight (HID) fadeometer is a standard 100 KLux instrument for fading experiments.[5] It is essentially a light box with a spherical inner surface for sample mounting, containing a normal atmosphere that has regulated temperature and humidity. The light source is a high power xenon arc lamp which is placed in the centre of the sphere, and is filtered accordingly to mimic as closely as possible the spectral profile of sunlight. Samples are placed equidistant from the lamp on the inner spherical sphere surface, which rotates around the light source to eliminate any radial non-uniformity in the output of the lamp. Sample absorption spectra were recorded at weekly intervals on a Hewlett Packard HP89532A diode array spectrophotometer.

A comparison of the spectral irradiance curves from the rapid fadeometer and the HID fadeometer, in Fig. 3, shows that a sample in the HID fadeometer experiences approximately 50× less light than the rapid fadeometer, which results in fading experiments taking weeks rather than hours to perform.

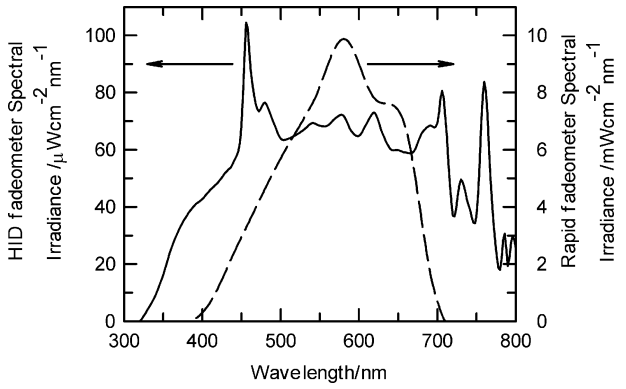

Fig. 3 Spectral irradiance curves of HID and rapid fadeometer.

Sample preparation

The method that is employed for this study uses a concentrated solution of dye in a suitable solvent system to create two samples that have a difference in SA : V ratio of 20 : 1.‡ The first is a thin film of concentrated dye in a poly(vinyl acetate)–dicyclohexylphthalate solvent mixture coated on a substrate, which has a constant SA : V ratio, since there are only two active interfaces separated by a small path length. The second is a coating of the same dye in the same solvent–polymer system which is dispersed in gelatin, with a similar absorbance to that of the film sample. By keeping the concentration of the dye in the oleophilic solvent identical to that in the film and subjecting both samples to an intense light source, the quantum yield of fade of both sample types can be directly compared and from it the effect of the significance of the oil/aqueous interface can be examined.

This method for comparing the fade characteristics of interfacial and bulk dye molecules is preferred, to say, making a range of dispersion coatings with different surfactants to change the size, and hence the SA : V ratio, of the oleophilic droplets. The Poissonian droplet size distribution is broad and using different surfactants will not induce changes in size significant enough to observe substantial differences in the rates of fade of dyes at the interface compared with the droplets-*versus*-film strategy of our experiment.

Although the samples described here are not truly representative of photographic coatings, the study was only a comparison of fade characteristics of the dyes in the vicinity of the interfacial region with those in the bulk droplet, in the absence of all other effects.

Therefore, as a sample form, a single layer coating containing a dispersion of preformed photographic dye in a coupler solvent was preferred to a multilayer photographic coating, where the dyes would be generated photographically. This sample form provided a physically analogous environment, but without the complication of the presence of residual chemistry following processing, arising not only from the colour layer of interest, but also from the adjacent layers.

The chosen solvent, dicyclohexylphthalate (DCP), is a particularly viscous member of the phthalate class, representative of coupler solvent classes used by the photographic industry. This solvent is crystalline at room temperature but can be melted and coated onto glass or quartz substrates as a film, as well as dispersed in gelatin with a suitable surfactant. But under an intense light source the solvent melts making it unsuitable for photobleaching experiments. However, using a 1 : 1 (w/w) mix of DCP with poly(vinyl acetate), PVAc, leads to films that are able to withstand intense light sources, and which can also be dispersed in gelatin. The absorbed light dissipated as heat in the sample may be removed by water cooling the reverse side of the substrate.

Non-oxidative fade experiments

Dispersion coatings. A concentrated dye solution was prepared by warming (50 °C) the relevant dye, DCP and PVAc (30 mg, 65 mg, and 65 mg, respectively) in butyl acetate

‡ Assuming a photographic coating contains spherical oil droplets of average radius of 0.15 μm, this leads to a SA : V ratio of 2×10^7 m^{-1}. For a film coating with concentration of dye at 0.25 M, absorption coefficient of 50 000 M^{-1} cm^{-1}, and a maximum absorbance of 1, this give a pathlength of approximately 1×10^{-6} m. The film has a single accessible surface A, and so the total volume is $A \times 1 \times 10^{-5}$, which leads to an SA : V ratio of 10^6 m^{-1}. This leads to dispersion samples possessing a SA : V ratio of approximately 20× greater than film samples.

(3 cm^3). 1.5 cm^3 of this dye solution was added dropwise to a warmed di-isopropyl naphthalene sulfonic acid, DPNS, surfactant (0.75% v/v) gelatin (5% w/w) solution, and mixed thoroughly. The coarse dispersion was then subjected to sonication for approximately 5 min before total frothing occured, and then stirred continuously on the water bath until all residual butyl acetate evaporated. Dispersion coatings with maximum absorbance of approximately 1 were fabricated by coating the warm dispersion solution (0.2 cm^3) with a warm aluminium plate across polished faces of clean quartz cuvettes (1 cm pathlength). The coatings were dried and stored in the dark at ambient temperature until required for use.

Thin film coatings. Thin films were fabricated by spreading gently the warmed concentrated dye–DCP–PVAc solution (0.2 cm^3) across polished faces of clean quartz cuvettes (1 cm pathlength). Once all the butyl acetate evaporated, a uniform thin film with a maximum absorbance of approximately 1 was achieved. The films were dried at room temperature before applying an overcoat of gelatin (5% (w/w) gelatin, 0.75% (v/v) surfactant solution).

The composition ratio of dye and DCP in film and dispersion samples was confirmed by HPLC measurements by using a methanol–acetonitrile–acetic acid–water (60 : 25 : 6 : 9 (v/v)) to extract both components from film and dispersion samples. This extraction mixture was passed through a reverse phase silica column, with a mobile phase of acetonitrile/water (98 : 2 v/v). The ratio of peaks heights suggested a 20% loss of dye in dispersion samples compared with film samples for both dyes, suggesting that although ballasted some dye escapes from the oil phase during sonication in the dispersion preparation.

Oxidative fade samples

Dispersion coatings and thin films were fabricated on glass microscope slides using the same coating techniques described above.

Analysis of absorption spectra

Multiple even derivative sharpening (MEDS). Two methods were used to analyse the absorption spectra of the dyes in film and dispersion coatings. The first was multiple-even derivative sharpening, MEDS, which utilises derivative-spectroscopy to extract weak underlying absorption bands.[23] Briefly, the method consists of a linear combination of even-derivatives to extract the overlapping bands without introducing extraneous features, which is the inherent disadvantage of using only the second-order derivative of a spectrum for analysis. MEDS was applied to each individual absorption spectrum to ascertain the number of underlying components.

Principal component analysis (PCA). The second method used was PCA,[24] a matrix based statistical tool which has been used to analyse overlapping bands in absorption spectra[25,26] as well as those in chromatography.[27] The method is more powerful with a large array of data sets, where each data set contains varying degrees of the same principal components. In that respect, it is ideal for a global analysis of fade data, which was preferable for the quantitative aspects of this study.

The software used to perform PCA was a Microsoft® Excel Add-In called *XLSTAT 4.4* written by Thierry Fahmy, and the third derivative of a factor indicator function was used to determine the number of significant principal components that account for all spectral features.[28] The data set used for each dye was a combination of the 9 absorption spectra recorded for film and dispersion samples during the non-oxidative fade experiments leading to a total of 18 absorption spectra for global analysis.

PCA was used in conjunction with MEDS to determine the number of components describing the absorption spectra of film and dispersion coatings. With any statistical fitting tool, n data points can always be fitted with an equation containing n parameters. Therefore, for sensible interpretations of the data, the number of significant principal components that account for all observations, r, should not approach n; indeed, from our experience the safe upper-limit is $r = n/3$.

Spectral fitting

Once the number of absorbing species in the photographic coatings was ascertained, the spectra were fitted using an asymmetric Gaussian function, described by a convolution of a hypsochromic, $F_h(\nu)$, and a bathochromic lineshape, $F_b(\nu)$. A is the amplitude of the Gaussian band, ν is energy in cm^{-1}, ν_0 is the energy at amplitude A.

$$F_h(\nu) = A \exp\left(-\log_e(2)\left(\frac{\nu-\nu_0}{\Delta\nu_h}\right)^2\right) \quad (15)$$

$$F_b(\nu) = A \exp\left(-\log_e(2)\left(\frac{\nu-\nu_0}{\Delta\nu_b}\right)^2\right) \quad (16)$$

An asymmetric function is preferred since in absorption spectroscopy an unresolved vibronic progression causes the appearance of an asymmetric absorption profile. It is known that many photographic dyes, especially PT dyes, show this asymmetry.

The absorption spectra for each fade set were analysed globally with linewidths and positions of bands fixed for all the spectra. Only the amplitudes were allowed to vary in the set, which provided a robust fit of the data. A least-squares minimisation procedure, based on the root-mean-square error, RMSE, function was used as the fitting routine.[29]

Antonov and Stoyanov[30] independently arrived at a similar algorithm for the analysis of absorption spectra by applying derivative spectroscopy to locate positions of features, and using an appropriate function to fit the spectra.

Calculation of quantum yields of fade

The quantum yields of fade were determined by interpolating the absorbance–time plots and calculating at incremental time intervals I_a and k_{loss} which both change during fade. By integrating the increments the quantum yield of fade was determined. To determine k_{loss} the values of ε_{max} for the dyes in dibutylphthalate were used since in DCP–PVAc this could not be determined accurately.

For aggregate absorption bands the quantum yields of fade assumed that the contribution to the total oscillator strength of a dye molecule residing within an aggregate is identical to that of one that exists solely as a molecular entity, *i.e.* the absorption coefficient per molecular unit at maximum absorbance is identical for all bands. This implies that individual dye molecules are destroyed, whether these reside within an aggregate or as separate entities, with the aggregate acting as a reservoir and fragmenting during photo-excitation.

Results and discussion

Rapid fade: a non-oxidative fade study

Fig. 4 shows the absorption spectra and MEDS analysis of film and dispersion coatings of dyes A and B. MEDS reveals 4 absorbing species in all samples, with 2 strong bands at *ca.* 500 and 545 nm and 2 smaller bands at *ca.* 425 and 625 nm being revealed for both dyes, suggesting aggregation in all samples.

PCA indicated a 4-component interpretation for the absorption spectra for dye A, which is consistent with the MEDS

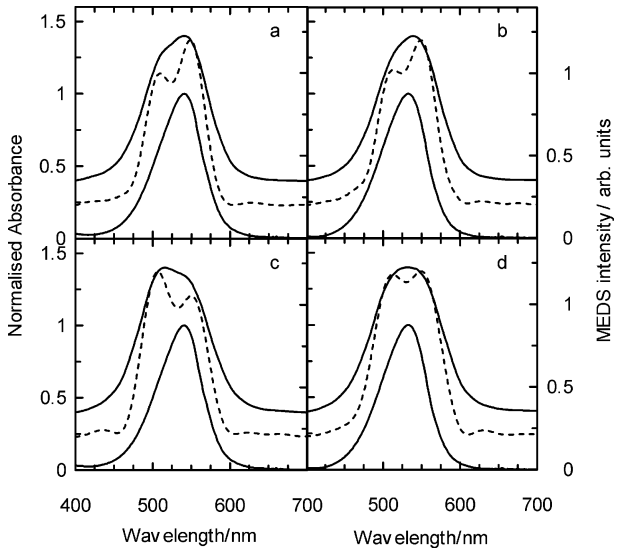

Fig. 4 Absorption spectra (line) and MEDS analysis (dashed) of (a) dye A dispersion, (b) dye B dispersion, (c) dye A film, (d) dye B film coatings. The lowest curves are the molecular absorption ban of the dyes in DCP–PVAc thin films (200 μM).

analysis, but for dye B it suggests an additional component not resolved by MEDS. This anomaly was investigated further by identifying the molecular absorption for each dye in the DCP–PVAc solvent system at a dilute concentration (200 μM)—these are offset in Fig. 4. The position of maximum absorbance of the molecular entity for dye A is extracted fairly well by MEDS analysis, but for dye B the molecular species remains unresolved in the face of a strongly ovelapping bathochromic feature. This supports the 5-component PCA result for dye B, with the additional component being attributed to the presence of *J*-aggregate absorption within 30 nm of the molecular entity band.

Although both MEDS and PCA suggested a 4-component fit for dye A coatings global spectral fitting of fade sets of both film and dispersion coatings of dye A preferred an additional absorption band bathochromic to the molecular absorption for statistically reproducible fits. Therefore dye fade data sets containing 18 absorption spectra of both film and dispersion coatings were analysed globally using 5 components, the parameters of which are presented in Table 1. The peak positions and hypsochromic and bathochromic half linewidths, HHW and BHW, respectively, were fixed for all the absorption spectra with only the amplitudes varying across the data set. Since the position and linewidth of the molecular entity absorption band are known for both dyes, these were fixed, with other bands positioned about this to describe the entire absorption envelope. Fig. 5 shows the behaviour of the amplitudes during fading for the 3 major bands.

Band 3 is the molecular absorption with bands 2 and 4 assigned as *H*- and *J*-aggregate absorption, respectively. As Table 1 shows these bands are narrower than band 3, which is consistent with the notion of the narrowing of the aggregate bands compared with those for molecular species.[31] Bands 1 and 5 are small relative to the 3 major bands and remain constant in amplitude throughout fade. They are either higher order *H*- and *J*-aggregates, artefacts caused by the digitisation of the absorption spectra, or low concentrations of absorbing impurities of the dyes. Regardless of the origin of these bands, they are small and remain relatively constant compared with the stronger bands, which fade much more significantly, and so are not relevant to any further discussion.

Fig. 5 shows that none of the species drops to less than 50% of their original values in the timescale of measurement. Dye B coatings possess a greater proportion of *J*-aggregates

Table 1 Parameters of the asymmetric Gaussian fit for non-oxidative fade study, in energetic units (cm^{-1}) and in wavelength (nm)

Band	Dye A							Dye B						
	A (%)[b]		Band position		Hypsochromic		Bathochromic		A (%)[b]		Band position		Hypsochromic		Bathochromic	
			ν_0/cm^{-1}	λ_{max}/nm	$\Delta\nu_h/cm^{-1}$	HHW/nm	$\Delta\nu_b/cm^{-1}$	BHW/nm			ν_0/cm^{-1}	λ_{max}/nm	$\Delta\nu_h/cm^{-1}$	HHW/nm	$\Delta\nu_b/cm^{-1}$	BHW/nm
1	7.3	(9.1)	21 500	465	1460	30	1005	23	6.5	(10.0)	21 400	467	1400	29	1100	26
2	16.1	(25.8)	19 930	501	950	23	840	22	8.7	(15.8)	19 800	504	820	21	750	20
3[a]	62.4	(49.3)	18 450	542	1550	42	845	26	56.1	(45.0)	18 800	532	1530	40	940	28
4	12.7	(12.4)	17 375	576	670	21	620	21	24.9	(22.3)	17 725	564	775	24	712	24
5	1.5	(3.4)	16 510	606	845	30	735	28	3.8	(6.9)	17 060	586	1262	40	1020	37

[a] Fixed by molecular absorption spectra. [b] Amplitudes for dispersion samples at $t = 0$, in brackets for film samples.

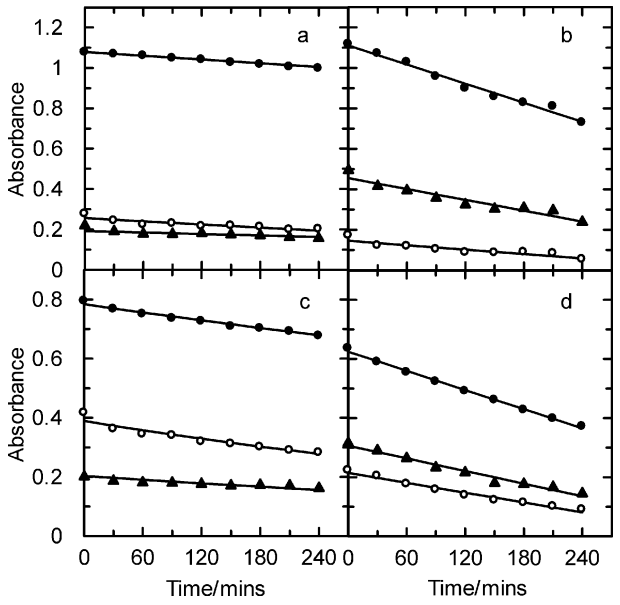

Fig. 5 Non-oxidative fade analysis of dispersion and film coatings of dye A (a and c) and B (b and d)—band 2 (unfilled circles), band 3 (filled circles), band 4 (filled triangles).

compared with dye A, which is consistent with previous studies on these dyes,[12] while dye A forms a greater proportion of *H*-aggregates. Moreover, the comparison demonstrates clearly that film samples of both dyes contain more aggregates than dispersion samples. This is caused by a small loss of dye during sonication when preparing dispersion samples.

Within the error of determination, bands 2, 3 and 4 decay linearly in absorbance. For the molecular species (band 3) where the starting absorbance is approximately 1, the initial rate of fade will be approximately constant, whereas for the aggregate species (bands 2 and 4), where the starting absorbances are much less than 1, the rate or fade will be proportional to species concentration. Quantum yields of fade for the individual bands are presented in Table 2 which show that in all samples, the *H*-aggregate absorption (band 2), has a larger quantum yield of fade than the molecular entity and *J*-aggregate absorption (bands 3 and 4, respectively). This can be explained by either accelerated photo-dissociation of the *H*-aggregates,[19] or by a simple chemical equilibrium between aggregates and molecular species.

Both types of aggregates are expected to be in dynamic equilibrium with molecular species, and when the latter are being photochemically destroyed, the equilibrium will counteract accordingly, leading to fragmentation of aggregates, and hence a loss in absorbance. This would lead to the quantum yield of fade for aggregate absorption bands being artificially large to maintain the molecular–aggregate equilibrium rather than destruction of aggregates through light fade. Consequently, the quantum yield of fade for the molecular species would be smaller than expected, since the equilibrium is always trying to replenish the faded molecular entities. However, the values for band 4 are similar to band 3, which suggests that the

Table 2 Non-oxidative fade results. Quantum yields of fade of dispersion and film samples

	$10^7\ \phi_{fade}$ (±25%)					
	Dye A			Dye B		
	Band 2	Band 3	Band 4	Band 2	Band 3	Band 4
Dispersion	1.1	0.4	0.4	2.5	2.2	1.7
Film	1.8	0.6	0.4	4.6	1.9	2.3

J-aggregate-molecular entity equilibrium is kinetically much slower in responding to any changes in concentration than the *H*-aggregate-molecular entity equilibrium. Nevertheless, trying to disassemble and quantify this is problematic and rather complex, and as the system will always try to maintain the dynamic equilibrium, the aggregates cannot be isolated from the molecular species.

What the values do show is that within experimental error the differences in SA : V ratio between film and dispersion samples of both dyes do not significantly affect the non-oxidative fade characteristics (in Table 2 see band 3 values for each case). As stated previously non-oxidative fade involves electron transfer and the formation of radical ion pairs. Therefore, depending on the redox potentials of specific electron transfer reactions, it is plausible that the aggregates of PT dyes may be able to shuttle electrons efficiently to and from surrounding aggregates and molecular entities to cause the destruction of the dye. It is understood that the mechanism of sensitisation of silver halide depends upon the efficiency of electron transfer from the excited state of the sensitising dye aggregates to the silver halide grains,[32–34] which suggests that dye aggregates could take part in a non-oxidative (electron transfer) fade mechanism. This is supported by the work of Furuya *et al.* who have shown that in dispersion samples the rate of dye fade can be suppressed by quenching the PT dye aggregate fluorescence with spiroindane derivatives.[8]

Kucybala *et al.* have focussed on the light stability behaviour of numerous magenta azamethine dyes in the presence of an electron donor, *N*-phenylglycine, in dilute ethyl acetate solutions.[7] The work also includes the study of a model PT dye and a value of ϕ_{fade} of 6.3×10^{-6} is estimated from their studies. This value is at least an order of magnitude larger when compared with those calculated here, but this difference is unsurprisingly owing to the presence of *N*-phenylglycine, which accelerates dye fade by approximately two orders of magnitude relative to a dilute solution of dye only.

HID fade: an oxidative fade study

With the presence of a normal atmosphere and longer overall fade times dye loss is now not limited by oxygen availability. Such conditions encourage an oxidative fade mechanism.

Using the positions of maximum absorbance and linewidths from Table 1, the oxidative fade results were analysed in a similar fashion to those of the non-oxidative fade experiments. Fig. 6 shows the results of the analysis with only the 3 major components shown for 3 sample types for each dye: a film coating, a dispersion coating, and a dispersion coating with an additional gelatin overcoat. The gelatin overcoat on the dispersion has the effect of acting as a barrier to reduce oxygen diffusion through to the dispersion coating, although Duxbury has shown that gelatin is still permeable to oxygen.[19]

In dispersions, Figs. 6a–d, the overall fade is rapid; each species falls to approximately half its initial concentration within the first 2 weeks. Fig. 6b shows that the dispersion without gelatin overcoat of dye B reaches this position within the first week. Within this timescale, the fade behaviour is similar to that in the non-oxidative fade study. The fade curves and the quantum yields of fade in Table 3 show that the presence of the gelatin overcoat uniformly reduces the quantum yields of fade of the 3 relevant species by 20–30%, by increasing the diffusion length of oxygen from the atmosphere to the dye in the dispersion.[35]

In contrast to the dispersion samples, the film samples of the two dyes, Figs. 6e and 6f, show a more distinctive behaviour. The film samples of dye B, Fig. 6f, are not much different from the corresponding dispersion samples, apart from the slightly slower initial fade rates, causing a "flattening" of the fade curves. However, for the film samples of dye A, Fig. 6e, the fade behaviour is more unusual. The initial fade rate of the

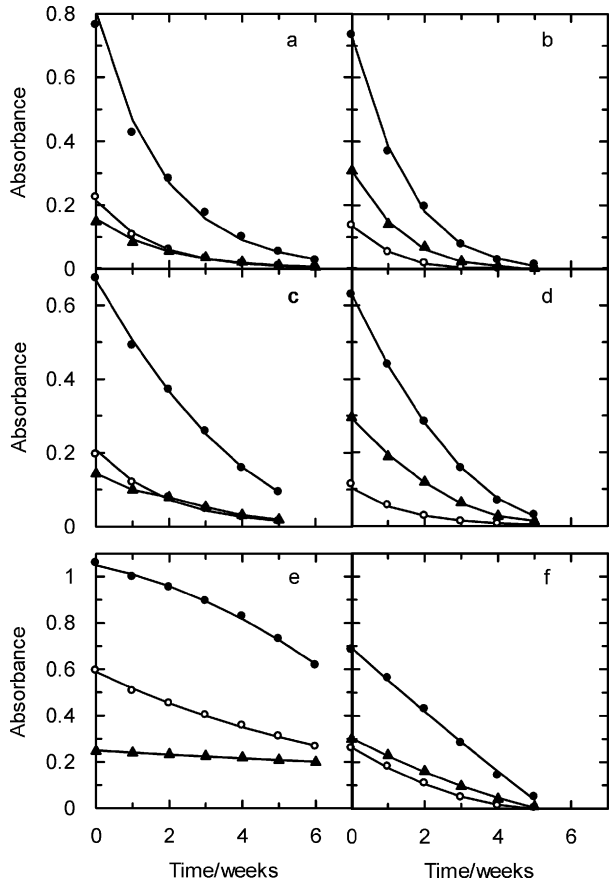

Fig. 6 Oxidative fade analysis of dispersions without gelatin overcoat, dispersions with gelatin overcoat and films of dye A (a,c,e) and B (b,d,f)—band 2 (unfilled circles), band 3 (filled circles), band 4 (filled triangles).

molecular species (band 3) is retarded, accelerating after 3–4 weeks, while the *J*-aggregate (band 4) shows an extremely slow fade rate.

The typically retarded fade behaviour exhibited by the molecular species is often explained by the presence of a sacrificial antioxidant. However, since both dispersion and film samples are made from the same parent oil it is difficult to identify such a species present in film samples but not in the dispersion samples. Our preferred explanation is that the *H*-aggregate of dye A decays upon excitation by first dissociating molecular entities. The relatively high initial concentration of *H*-aggregates provides a significant supplementary increase of the molecular species in the initial phase (0–3 weeks) of fade. Thereafter, the molecular species decay at a rate dominated by their own fade photochemistry. The value for this component, Table 3, dye A film, band 3, is determined on this assumption. Similar mechanisms have been proposed by others who have studied dye fading.[19,36] However, in addition to this disaggregation mechanism, it is tempting to speculate that a secondary effect derived from the concentration enhancement of the molecular species, in turn, supplements the *J*-aggregate (band 4), resulting in its unusually low quantum yield of fade.

Table 2 shows that the rapid disappearance of the *H*-aggregate is also observed to some extent in non-oxidative fade, which provides some evidence for fade quenching of the molecular species by the *H*-aggregates. However, as stated previously, re-equilibration between aggregates and molecular entities complicates the issue and cannot be separated, making it difficult to verify the hypothesis.

The oxidative fade results show that dye A film samples fade approximately twice as fast as the corresponding dispersion samples, implying that the different SA : V ratios affect the fade chemistry. However, although the results for dye B film samples suggest the same trend, these are not as clear-cut. This discrepancy between dye A and dye B is thought to be due to different aggregation/de-aggregation kinetics rather than different quantum yields of singlet oxygen production between the two dyes as this would not have any effect on the comparative fade performance in the different sample forms. Previous studies have shown that the formation of *J*-aggregates by dye B is much more facile in non-polar solvents and at oil/aqueous interfaces compared with dye A.[12] This is supported by inspection of the amplitudes of the individual components in Figs. 5 and 6. It is thus feasible that the aggregate–molecular entity equilibrium for dye B responds to changes in relative concentration better than dye A. During fade this would implicate a faster response by the aggregates of dye B to the loss of molecular entities compared correspondingly with dye A, where de-aggregation is the rate-determining step. This difference would manifest itself in greater loss of dye in coating samples of dye B compared with dye A, which is observed. As stated previously for non-oxidative fade, trying to isolate these different effects is problematic.

Overall, the results do indicate that dispersion samples show accelerated fade compared with film samples. Although the difference in the SA : V ratio between dispersion and film samples has been estimated to be a factor of 20, this has clearly not translated into the quantum yields of fade. There may be several reasons that cause this.

A number of groups have investigated oxidative dye fading and it has been recognised that in microheterogeneous media, such as dispersions, oxidative fade kinetics can be complicated by singlet oxygen being able to escape from the locus of generation.[37] In dispersions singlet oxygen formed may travel to other oil droplets through the aqueous gelatin phase prior to being quenched or deactivated. This makes oxidative fade in dispersions independent of the source of singlet oxygen production. It is generally agreed that the main factors governing it are the rate of diffusion through the sample, the concentration of oxygen at specific interfaces, and the ability for oxygen to penetrate those interfaces.[35,38,39]

For our oxidative fade results, we propose to explain the difference between film and dispersion samples using a kinetic model to describe oxygen diffusion through a coating containing different interfaces (Fig. 7). The model applies a simple

Table 3 Oxidative fade results. Quantum yields of fade of dispersion (with and without gelatin overcoat) and film samples

	$10^7\ \phi_{fade}$ (±25%)					
	Dye A			Dye B		
	Band 2	Band 3	Band 4	Band 2	Band 3	Band 4
Dispersion (without gelatin)	11.3	7.5	8.1	16.0	9.2	11.0
Dispersion (with gelatin)	9.7	5.2	5.8	13.3	6.8	8.1
Film	3.8	2.6[a]	0.7	11.3	5.0	6.5

[a] This is calculated after the first 4 weeks of fade.

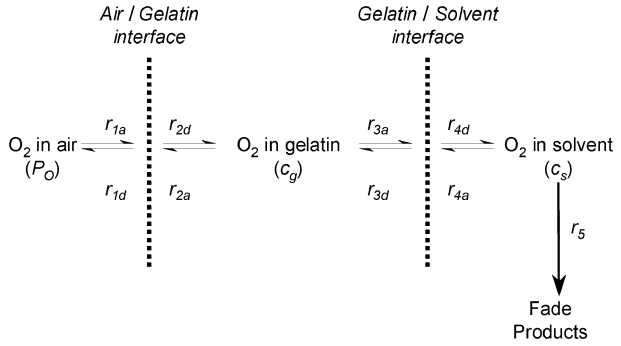

Fig. 7 Kinetic scheme of O_2 diffusion through coatings. P_O—partial pressure of O_2 in air; c_g, c_s—concentration of O_2 in gelatin and solvent respectively; r_a, r_d—rate of adsorption and desorption at each interface.

adsorption isotherm to describe the diffusion of oxygen through each interface, but excludes any consideration of singlet oxygen migration beyond individual solvent/droplet boundaries. From air, r_{1a} and r_{1d} are the rates of adsorption and desorption of oxygen at the air interface and are expressed simply as

$$r_{1a} = k_1 N_{ag}(1 - x)P_O \tag{17}$$

and

$$r_{1d} = k_{-1} N_{ag} x \tag{18}$$

where the equilibrium constant at the air/gelatin interface, K_1, is defined as

$$K_1 = \frac{k_1}{k_{-1}} \tag{19}$$

Here P_O is the partial pressure of oxygen in air, N_{ag} is the total number of vacant sites per unit area, x is the fractional occupancy of the vacant sites by oxygen, and k_1 and k_{-1} are the corresponding rate constants for adsorption and desorption at the air/gelatin interface.

From the gelatin, adsorption and desorption at the gelatin/air interface, the complimentary expressions are

$$r_{2a} = k_2 N_{ag}(1 - x)c_g \tag{20}$$

and

$$r_{2d} = k_{-2} N_{ag} x \tag{21}$$

where the equilibrium constant at the gelatin/air interface, K_2, is defined as

$$K_2 = \frac{k_2}{k_{-2}} \tag{22}$$

Similar expressions can be derived at the gelatin/solvent interface, to obtain r_{3a}, r_{3d}, r_{4a}, and r_{4d} which take an analogous form to eqns. (20) and (21). c_g and c_s are the respective concentrations of oxygen in gelatin and the solvent phase and together with N_{gs} vacant sites, and a fractional occupancy of y, yield the equilibrium constants K_3 and K_4.

This leads to the overall kinetic model expressed by eqns. (23)–(25).

$$\frac{\partial c_a}{\partial t} = r_{1d} - r_{1a} = k_{-1} N_{ag} x - k_1 N_{ag}(1 - x)P_O \tag{23}$$

$$\begin{aligned}\frac{\partial c_g}{\partial t} &= r_{2d} - r_{2a} + r_{3d} - r_{3a} \\ &= k_{-2} N_{ag} x - k_2 N_{ag}(1 - x)c_g + k_{-3} N_{gs} y - k_3 N_{gs}(1 - y)n_g\end{aligned} \tag{24}$$

$$\begin{aligned}\frac{\partial c_s}{\partial t} &= r_{4d} - r_{4a} - r_5 \\ &= k_{-4} N_{gs} y - k_4 N_{gs}(1 - y)c_s - k_5 c_s\end{aligned} \tag{25}$$

Here c_a is the concentration of oxygen in air and r_5 represents the rate of formation of dye fade products from the photochemical reaction of oxygen with the dye in its excited state. It should be noted that k_5 is an approximate rate constant and is actually a convolution of the concentration of ground state dye, photon flux and the intrinsic rate constant for the destruction of dye. However, since we are working in a near-steady state regime k_5 can be taken to be constant.

In the absence of illumination, $k_5 = 0$, the equilibrium concentration of oxygen in the organic phase is *ca.* 10× greater than in the aqueous gelatin phase[40] and the steady state concentrations of oxygen in the gelatin and solvent phases are given by:

$$c_s^0 = \left(\frac{K_3}{K_4}\right) c_g^0 = \left(\frac{K_3}{K_4}\right)\left(\frac{K_1}{K_2}\right) P_O \tag{26}$$

In the presence of constant illumination, $k_5 \neq 0$, new quasi-steady state concentrations of oxygen in the gelatin and solvent phases are established. In the solvent phase this takes the form:

$$c_s^{eq} \approx \left\{ A + B\left(\frac{k_5}{N_{ag}}\right) + C\left(\frac{k_5}{N_{gs}}\right) \right\}^{-1} \tag{27}$$

where

$$A = \frac{1}{c_s^0} \tag{28}$$

$$B = \left(\frac{1}{K_4 c_s^0} + 1\right)\left(\frac{1}{k_{-2}}\right) \tag{29}$$

and

$$C = \left(\frac{1}{K_4 c_s^0} + 1\right)\left(\frac{1}{k_{-3}} + \frac{1}{k_{-4}}\right) \tag{30}$$

This leads to a particularly clear expression for the rate of fade:

$$r_s = \left\{ \frac{A}{k_5} + \frac{B}{N_{ag}} + \frac{C}{N_{gs}} \right\}^{-1} \tag{31}$$

Under weak illumination conditions, it is expected that the *A*-term dominates this expression, whilst at very high intensity illumination it becomes insignificant compared with the *B*- and *C*-terms. The experience in the photographic industry is that HID conditions offer something of a compromise between allowing a linear dependence of fade rate *vs.* intensity in dispersion coatings (*A*-term dominant) and the shortest reasonable duration for fade testing purposes (*B*- and *C*-terms dominant), where a bottleneck at either the air/gelatin or gelatin/solvent interfaces may become apparent. In reality, these terms may all be of the same order.

In the film coating (where $N_{ag} \approx N_{gs}$), if reasonable assumptions about the relative magnitudes of k_{-2}, k_{-3}, and k_{-4} are made the *A*-, *B*- and *C*-terms will all provide roughly equal contributions to the rate of fade. The dispersion coating contains the same number of dye molecules per unit area as the film coating since both have the same optical density, but the SA : V ratio at the gelatin/solvent interface is greater in the dispersion case by a factor of *ca.* 20. Consequently, N_{gs} increases by the same amount, so that only the *A*- and *B*-terms will be significant.

The characteristics of this model thus show that, all other things being equal, increasing the gelatin/solvent interfacial area will lead to an increase in fade rate, but not directly in proportion. Our experimental results are consistent with this

model, and show that in spite of an increase of *ca*. 20 in N_{gs} going from film to the dispersion sample, only a corresponding factor of 1.5 to 2 increase in the rate of dye fade is observed.

The model can also be used to explain the difference in the quantum yields of fade between dispersion coatings of dye A and dye B, where only the *A*- and *B*-terms are significant. Previous studies of the photophysical properties of the two dyes strongly suggest that k_5 for dye B is approximately a factor of 2 to 3 larger than that for dye A.[12] If the *A*-term and *B*-term are of the same order of magnitude then this translates into only a factor of approximately 1.3 difference in r_5 between the two dyes, which is observed. However, the comparison between the dyes in the film-coatings is not as clear-cut due to the unusual retardation in the initial fade rate of dye A.

Furthermore, the kinetic model shows that provided that the *A*-term is comparable with the *B*-term at HID intensities, and the *C*-term is smaller than either owing to the increased SA : V at the gelatin/solvent interface in a dispersion situation, then the rate determining step for dye fade starts to become the migration of oxygen through the air/gelatin interface.

Conclusions

We have investigated the effect of increasing the SA : V ratio of the solvent/gelatin interface on the light stability of dyes dispersed in single-layer gelatin coatings. Two dyes (dyes A and B) were studied in conditions designed to favour both non-oxidative fade and oxidative fade.

The non-oxidative fade study demonstrates that in the absence of oxygen a non-oxidative fade mechanism involving both aggregates and molecular entities of the dyes is established in high concentration environments. It shows that increasing the SA : V ratio of the solvent/gelatin interface when going from film to dispersion coatings, does not yield a significant difference in the non-oxidative fade characteristics of the dyes. The study also shows that dye B possesses a quantum yield of non-oxidative fade that is approximately a factor of 3 greater than that for dye A, which is a manifestation of the relative difference between the singlet excited state lifetimes of the dyes.[12]

The oxidative fade study reveals that PT dyes possess a dominant oxidative fade mechanism compared with the non-oxidative alternative. The study has shown that the difference in photophysical properties of dyes A and B does not fully translate to the quantum yield of oxidative fade. However, more importantly, it has shown that there is only a factor of 1.5 to 2 difference between the quantum yields of fade of the dyes in dispersion and film samples, which is smaller than expected from simple SA : V ratio considerations. Both observations can been explained by applying a kinetic model based on a simple adsorption isotherm to the diffusion of oxygen through film and dispersion coatings. Moreover, our results and kinetic model are consistent with the onset of a bottleneck to oxygen diffusion at the air interface which prevents changes in k_5 and/or N_{gs} from being fully transferred to the quantum yield of fade.

Acknowledgements

The authors wish to thank the Engineering and Physical Sciences Research Council (EPSRC) for financial support. C. K. Parmar also wishes to thank Kodak European Research for an EPSRC CASE studentship, as well as P. Halligan, W. Landon, and D. Lewis at Kodak European Research for performing the HID and HPLC measurements.

References

1 H. Wilhelm, in *International Association of Fine Art Digital Printmakers Meeting*, Wilhelm Imaging Research Inc., New York, March 1999–updated June 2000, http://www.wilhelm-research.com/pdf/WIR_Permanence_06_2000.pdf.
2 H. Wilhelm and C. Bower, *The Permanence and Care of Color Photographs – Traditional and Digital Color Prints, Color Negatives, Slides and Motion Pictures*, Preservation Publishing Company, Grinnell, 1993.
3 P. Gregory, *Chem. Brit*., 2000, **36**, 39.
4 J. R. Thirtle, *Principles and Chemistry of Color Photography, in The Theory of the Photographic Process*, ed. T. H. James, Macmillan Publishing Co. Inc., New York, part I, ch. 12, 1977.
5 W. F. Smith, W. G. Herkstroeter and K. L. Eddy, *Photogr. Sci. Eng*., 1976, **20**, 140.
6 T. Kurosaki, S. Itamura, S. Rokutanda, T. Teramoto and T. Miyagawa, *J. Photogr. Sci*., 1988, **36**, 79.
7 Z. Kucybala, I. Pyszka, B. Marciniak, G. L. Hug and J. Pasczkowski, *J. Chem. Soc., Perkin Trans. 2*, 1999, 2147.
8 K. Furuya, N. Furutachi, S. Oda and K. Maruyama, *J. Chem. Soc., Perkin Trans. 2*, 1994, 531.
9 R. J. Tuite, *J. Appl. Photogr. Sci. Eng*., 1979, **5**, 200.
10 J. Bailey, *J. Chem. Soc., Perkin Trans. 1*, 1977, 2047.
11 P. Douglas, S. M. Townsend, P. J. Booth, B. Crystall, J. R. Durrant and D. R. Klug, *J. Chem. Soc., Faraday Trans*., 1991, **87**, 3479.
12 C. K. Parmar, G. Rumbles and C. J. Winscom, *Phys. Chem. Chem. Phys*., 2002, **4**, 1766.
13 D. T. Sawyer and R. J. P. Williams, *Oxygen Chemistry*, Oxford University Press, Oxford, 1991.
14 A. A. Gorman and M. A. J. Rogers, *Chem. Soc. Rev*., 1981, **10**, 205.
15 R. J. Berry, P. Douglas, M. S. Garley, T. Jolly, D. Clarke, H. Moglestue, H. Walker and C. J. Winscom, *J. Photochem. Photobiol., A*, 1999, **120**, 29.
16 W. F. J. Smith, W. G. Herkstroeter and K. L. Eddy, *J. Am. Chem. Soc*., 1975, **97**, 2764.
17 P. Douglas and D. Clarke, *J. Chem. Soc., Perkin Trans. 2*, 1991, 1363.
18 P. Douglas, S. M. Townsend and R. Ratcliffe, *J. Imag. Sci*., 1991, **35**, 211.
19 D. F. Duxbury, *Dyes Pigm*., 1994, **25**, 131.
20 A. A. J. Krasnovskii, Y. A. Venediktov and O. M. Chernenko, *Biophys*., 1982, 1009.
21 P. Douglas, *J. Photogr. Sci*., 1988, **36**, 83.
22 T. Aono, K. Nakamura and N. Furutachi, *J. Appl. Photogr. Eng*., 1982, **8**, 227.
23 C. J. Winscom, D. Clarke, C. K. Parmar and G. Rumbles, submitted.
24 M. Kubista, J. Nygren, A. Elbergali and R. Sjoback, *Crit. Rev. Anal. Chem*., 1999, **29**, 1.
25 N. Ohta, *Anal. Chem*., 1973, **45**, 553.
26 R. M. Wallace, *J. Phys. Chem*., 1960, **64**, 899.
27 S. Wold and M. Sjostrom, *Acta Chem. Scand*., 1998, **52**, 517.
28 A. Elbergali, J. Nygren and M. Kubista, *Anal. Chim. Acta*, 1999, **379**, 143.
29 J. F. Kenney and E. S. Keeping, Root Mean Square, in *Mathematics of Statistics*, ed. V. Nostrand, Princeton, USA, 1962, p. 59.
30 L. Antonov and S. Stoyanov, *Appl. Spectr*., 1993, **47**, 1030.
31 M. Kasha, *Rad. Res*., 1963, **20**, 55.
32 W. West and P. B. Gilman, Jr, in *The Theory of the Photographic Process*, ed. T. H. James, Macmillan Publishing Co. Inc., New York, ch. 10, 1977.
33 J. M. Lanzafame, A. A. Muenter and D. V. Brumbaugh, *Chem. Phys*., 1996, **210**, 79.
34 M. T. Spilter, A. Ehret, R. Kietzmann and F. Willig, *J. Phys. Chem. B*, 1997, **101**, 2552.
35 C. H. Giles, C. D. Shah, D. P. Johari and R. S. Sinclair, *J. Soc. Dye Colour*, 1972, 59.
36 R. Nakamura and M. Hida, *Sen-i Gakkaishi*, 1983, **39**, T-125.
37 E. A. Lissi, M. V. Encinas, E. Lemp and M. A. Rubio, *Chem. Rev*., 1993, **93**, 699.
38 L. Palchetti, Q. Li, E. Giorgetti, D. Grando and S. Sottini, *Appl. Opt*., 1997, **36**, 1204.
39 P. R. Unwin, C. J. Slevin, S. Ryley and D. J. Walton, *Langmuir*, 1998, **14**, 5331.
40 *CRC Handbook of Chemistry and Physics*, ed. D. R. Lide, CRC Press, Boca Raton, FL, USA, 76 edn., 1995–1996.